JOURNAL OF Applied Polymer SCIENCE

Improving adhesion between aramid fibers and natural rubber through morphological and synthetic modification of the fibers

Nihal Kanbargi, Alan J. Lesser
Department of Polymer Science & Engineering, University of Massachusetts, Amherst Massachusetts 01003
Correspondence to: A. J. Lesser (E-mail: ajl@polysci.umass.edu)

ABSTRACT: In this article, we present new methods to improve the adhesion between poly(paraphenylene terephthalamide) fibers and a natural rubber for tire reinforcement. Fiber pretreatments are applied to create new surface morphologies on the fiber that enables enhanced adhesion between the fiber and rubber matrix. The pretreated fibers are then subject to treatments with coupling agents in the presence of supercritical carbon dioxide ($scCO_2$) in an attempt to permeate the fiber surface and chemically bind the fiber to the rubber matrix. Shear lag analysis using a Kelly Tyson approach is compared to more refined models to evaluate optimum test parameters for fiber pull-out adhesion tests. The results show that the adhesion increases by approximately 100% when compared to conventional composites. Failure analysis of fiber surface reveals a suppression of interfacial failure. The effects of pretreatments on fiber properties are also characterized, and the optimization between fiber properties, fiber–matrix interface properties, and overall composite properties are discussed. © 2017 Wiley Periodicals, Inc. J. Appl. Polym. Sci. **2017**, *134*, 45520.

KEYWORDS: composites; crosslinking; mechanical properties; structure–property relationships

Received 26 May 2017; accepted 10 July 2017
DOI: 10.1002/app.45520

INTRODUCTION

Poly(paraphenylene terephthalamide) (PPTA) reinforced long fiber composites have been used for a variety of applications including aerospace, automobiles, and personal protection in soft body armors for ballistic protection. First introduced by Dupont in 1971 as Kevlar, PPTA fibers (also known as Twaron or Technora) have gained widespread use due to their extraordinary high modulus and tensile strength.[1] These properties have been attributed to its molecular structure and fiber microstructure.[2–6] However, the strength of composites prepared from PPTA fibers is largely limited due to poor interfacial adhesion between the fiber and matrix.[7–9] Inadequate adhesion between the fiber and matrix limits the overall performance of the composite since the high strength of the fiber is not realized in these applications due to premature interfacial failure.

Various approaches have been studied to improve the adhesion of PPTA fibers to various matrices with little or no improvement. Most of them have involved functionalizing the surface[10–17] to generate chemical interaction with the corresponding matrix. Some treatments also introduce fiber roughness.[11,18] Additional techniques have also involved dip-coating the fibers in adhesives.[19] However, the aromatic nature of the backbone and the physical microstructure of the PPTA fiber make it more difficult to form fiber–matrix covalent bonds as compared to glass or carbon fibers[20] thereby limiting the potential performance of composites using this class of fiber.

Herein, we report a new strategy to improve composite performance by first, altering the fiber surface morphology to allow for penetration of reactive monomers into the fiber subsurface, and second, treatment of these reactive monomers to enable covalent bonding to occur on the fiber surface and within its subsurface when the rubber matrix is cured (vulcanized). A necessary part of our strategy is to compromise some of the PPTA fiber properties from the applied pretreatments to allow for significantly increased load transfer from the rubber matrix, thereby enhancing the composite performance. It should be noted that the specific methods employed herein to modify the fiber through pretreatments are tailored for this composite system, but the general concept of modification of the interphase region is quite general and can apply to other composite systems as well. These treatments have been patented by Bridgestone, America[21] and the supporting research is described in this communication.

EXPERIMENTAL

Experimental Overview

The fiber pretreatments are selected to promote enhanced surface area and subsurface area in the fiber itself to allow for

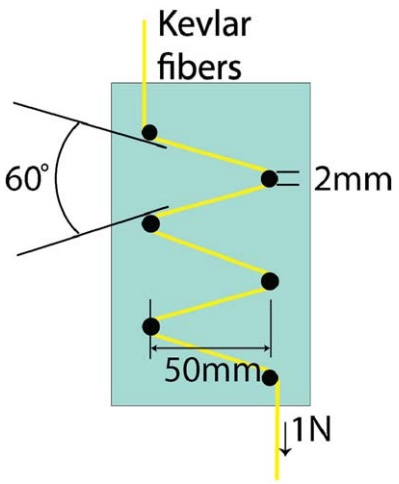

Figure 1. Mechanical treatment setup. [Color figure can be viewed at wileyonlinelibrary.com]

better transfer of coupling agents into the fiber interphase regions using supercritical carbon dioxide ($scCO_2$). Two pretreatment methods that change the surface morphology of the fibers are reported in this communication. The first pretreatment is chosen to exploit the subsurface nanovoids present in these fibers while the other takes advantage of the relatively weak compressive properties of the fiber.[22] It is acknowledged that a drop in fiber properties due these treatments is expected, but ultimately this is acceptable because the treatments enhance the interfacial adhesion between the fiber and matrix and improve overall composite performance.

After the pretreatment step, fibers are treated with reactive monomers to chemically bind the fiber surface and subsurface to the rubber matrix. The reactive monomers reported herein are selected based on their ability to take part in the crosslinking mechanism and potentially increase the crosslinking density of the rubber matrix in the fiber interphase region.

Finally, test samples were fabricated by curing the rubber matrix in the presence of the fibers to create test specimens necessary for evaluation of adhesion.

Materials

PPTA fibers (840 denier, 534 filaments) were obtained from Dupont Chemicals Co and used as is. Uncrosslinked natural rubber (poly(*cis*-isoprene)) latex with sulfur premixed as crosslinker was provided by Bridgestone America and used as the matrix.

Fiber Pretreatments

PPTA fibers were subject to two morphological pretreatments. Two pretreatments are considered; a mechanical pretreatment and a microwave pretreatment.

PPTA fibers are known to be weak in compression.[22,23] Elastica[24] tests performed on the fibers have shown that the fibers deform in a non-Hookean manner at very low bending strains and this deformation is plastic in nature.

To exploit this property and create buckling on the fiber surface, a simple setup is used on the Instron 5500R tensile testing machine to induce compression on the fiber surface (see Figure 1). Metal cylinders of diameter 2 mm were embedded in a wooden frame in a zigzag fashion as shown in Figure 1. One end of the fiber bundle was tied to a weight of 0.1 kg, weaved over the metal cylinders and the other end secured to the Instron tensile testing machine. The Instron was used to pull the fiber bundle at a crosshead speed of 500 mm/min to induce compression by bending of the fiber surface.

The second pretreatment involves the use of microwaves. In other applications, microwave radiation has been used to create finely divided graphite using sulfuric acid.[25] In this process, graphite is first soaked in an intercalating agent (sulfuric acid). Next, the chemical is vaporized by subjecting it to microwaves volatilizing the acid and subsequently forcing rapid expansion and exfoliation of graphite platelets. A similar approach is used to open up PPTA fibers since trace levels of sulfuric acid are already known to be present within the subsurface voids of the fiber (a consequence of the dry-jet wet-spinning process). Since there is an affinity of sulfuric acid to the voids for PPTA fibers, a soak in 50% sulfuric acid for a period of 1 h at room temperature is carried out prior to subjecting the fibers to microwaves. The fibers are then placed in a test tube, immersed in water, and treated to microwaves in a CEM Discover SP microwave synthesizer to volatilize and exfoliate the fiber surface. The microwave conditions were fixed at 100 W for 2 min. The fibers were then washed and dried to be used for study. The effect of these pretreatments on the properties of the fiber was studied using single fiber tests and small-angle X-ray scattering. Fiber morphology was studied using scanning electron microscopy. Scanning electron microscopy was performed either using a FEI Magellan 400 FESEM or a JEOL JCM-5000 SEM. Small-angle X ray scattering was performed using a Ganesha SAX-LAB instrument.

Tensile tests on the single fibers were performed using an Instron Tensile testing machine equipped with a 50 N load cell. Prior to testing, single fibers were mounted using a 3 *M* general purpose commercial grade epoxy on a rectangular cardboard frame with a smaller rectangular hole having a gauge length of 50 mm. The frame containing the fiber was then mounted onto the test machine grips. Next, the frame was cut on both sides at appropriate places. Finally, the fiber was then tested in tension at crosshead speed of 1 mm/min until failure. A minimum of 10 fibers were used for each condition.

The pretreated fibers are then soaked in reactive monomers. The soak was carried out both in the presence of $scCO_2$ and in ambient conditions. Carbon dioxide of purity grade $>99\%$ was obtained from Airgas and used as is. In addition reactive monomers were considered; divinyl benzene (DVB) (80%) and tetramethyl-tetravinyl-cyclotetrasiloxane (D4V) (90%), both of which were obtained from Sigma Aldrich and used as is without dilution. The choice of coupling agents is explained in the Results and Discussion section. After pretreatment, PPTA fiber bundles were place in test tubes and filled with coupling agents. Ambient condition soak was performed wherein fiber bundles

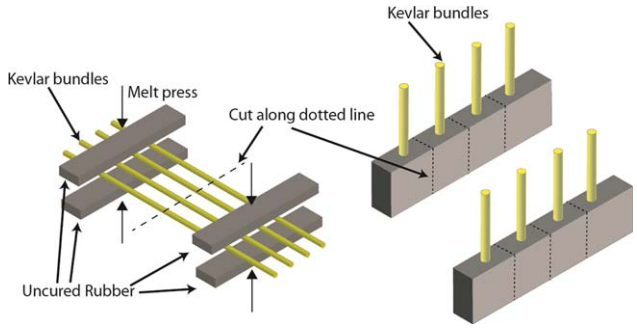

Figure 2. Fabrication of composites for adhesion tests. [Color figure can be viewed at wileyonlinelibrary.com]

were soaked in coupling agents at room temperature and pressure for a duration of 1 h. The test tubes were placed in high pressure reactors for the soak in $scCO_2$. Carbon dioxide was pumped into the reactors to a pressure of 34.5 MPa using a Thar Designs P200 high pressure pump. The reactor was then heated to 50 °C and maintained for 1 hour. Afterward, depressurization was carried out in 1–2 s. Test specimens for fiber matrix adhesion studies involved first fabricating test specimens (see Figure 2). It should be noted that the embedded length used in the adhesion test geometry shown in Figure 2, was determined from a shear lag analyses (described in the discussion of results and Appendix A) to insure uniform stress distribution across the fiber length. The fabrication process first involves placing fiber bundles between strips of uncured rubber followed by curing of the rubber together with reactive monomers under pressure and temperature. Fiber bundles were first subject to a fixed amount of twist (150 turns/m) so that the fiber bundles presented a uniform surface area to the matrix. The rubber curing was done for 20 min at a temperature of 160 °C following recommendations from Bridgestone.

The fiber composite test specimens were then secured using a special setup on the Instron 5500R Tensile testing machine with a 10 kN load cell. The setup ensured a restrained top loading condition on the rubber matrix. The fiber bundle was then pulled until failure, that is, the fiber bundle was completely pulled out of the rubber matrix. Adhesion tests were performed on various combinations of pretreatments and coupling agents. A minimum of five samples were used for each type of treatment. Fracture surfaces from the pull-out tests were observed under the SEM to determine the mode of failure.

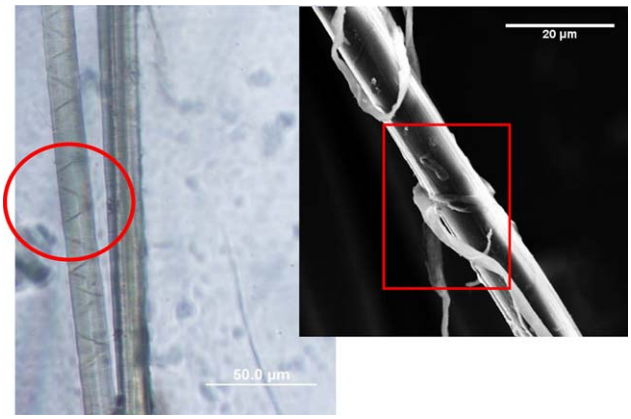

Figure 4. Optical (left) and scanning electron microscopy (right) images of mechanical treated fibers show "v" shaped kink bands (encircled) and fibrillation (boxed). [Color figure can be viewed at wileyonlinelibrary.com]

RESULTS AND DISCUSSION

Fiber Pretreatments

PPTA fibers are processed using a dry-jet wet-spinning process, which leads to extremely high molecular anisotropy. Detailed studies have shown that PPTA fibers have a pleated structure where lamellae are stacked in a radially oriented fashion.[2,3] Interlamellar hydrogen bonding and high crystallinity are found to be contributors to the fiber's strength.[26] An important characteristic that results from the dry-jet wet-spinning is the presence of subsurface nanovoids[27] caused due to the entrapment of traces of sulfuric acid (solvent). These nanovoids are further exploited to develop enhanced subsurface voids and fiber texture using microwave radiation.

As detailed in the Experimental section, PPTA fibers that are initially soaked in sulfuric acid followed by exposure to microwave radiation produces interesting subsurface blisters (see Figure 3). This blister pattern arises from volatilized acid initially embedded between the "onion skin" morphology present in the PPTA fibers.

The mechanical pretreatment to the PPTA fiber, also detail in the Experimental section, is designed to take advantage of the

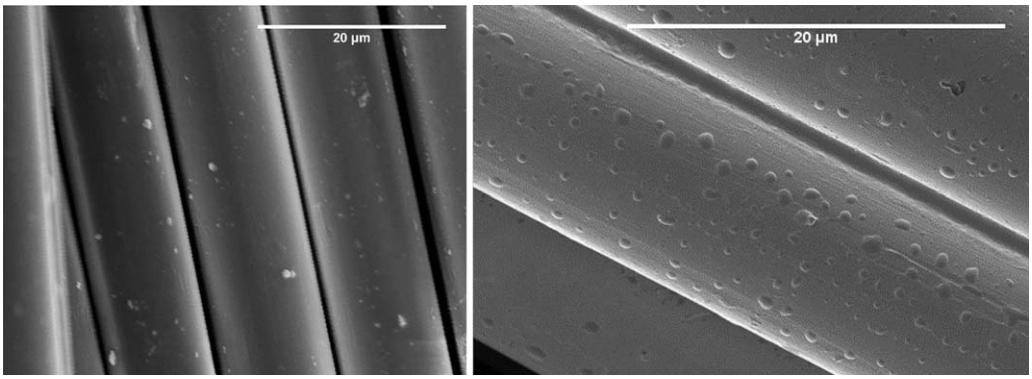

Figure 3. Scanning electron micrographs of untreated fibers (left), compared to the microwave treated fiber (right). Note the subsurface blister pattern produced on the fiber resulting from the treatment.

Table I. Void Sizes Obtained from Guinier Analysis on Small-Angle X-Ray Data

Treatment	Void size (nm)	R^2
Control	54	0.97
Mechanical	56	0.97
Microwave	46	0.96

relatively weak compressive properties of the fiber and promote increased surface area resulting from the formation of kink bands and delamination of fiber. It is acknowledged that both these pretreatments cause loss in strength and modulus, as shall be quantified, but is ultimately acceptable to improve overall mechanical properties of the composite. Optical microscope and SEM images show, typical evidence for buckling under compression, that is, "v" notches or kink bands and fibrillation (Figure 4).

Small-angle X-ray analysis was conducted on fibers after both pretreatments were applied to identify if any subsurface area was created at that length scale. Performing Guinier analysis (see Appendix B) on small-angle X-ray scattering data[27] indicates that the sub surface voids have not changed in size (Table I). Therefore, it seems that the pretreatments do not affect the voids in a measurable way but serve to change the surface morphology or texture significantly.

Single fiber fragmentation tests were performed as described in the Experimental section. The results are in Figure 5.

For the treatment parameters chosen, tensile strength and modulus for the treated fibers are quantified in terms of values of control fibers in Table II. The treatment conditions have not been optimized, so fine tuning of these treatments can be done to minimize the damage on the fibers.

Note that the mechanical treatment has a more significant effect on the modulus rather than the strength when compared to the microwave treatment process. This arises from the fact that the mechanical treatment primarily causes in increase in internal surface area that results primarily in softening of the fiber. In

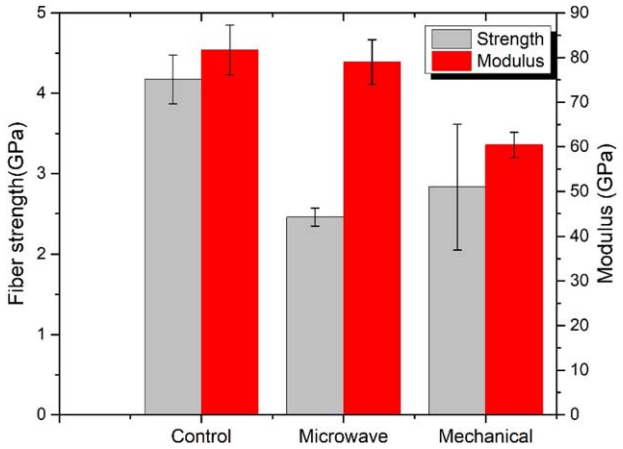

Figure 5. Effect of pretreatment on the fiber stiffness and strength. [Color figure can be viewed at wileyonlinelibrary.com]

Table II. Properties of Treated Fiber Expressed as Percentage of Control Fiber

	Tensile strength (%)	Modulus (%)
Microwave	59	97
Mechanical	68	75

contrast, the microwave treatment can cause significant degradation through chain scission, which in turn, results in losses to fiber strength where modulus is relatively insensitive.[28,29]

Reactive Monomer Infusion

Two reactive monomers were selected for this study; a low molecular weight silicone tetramethyl-tetravinyl-cyclotetrasiloxane (D4V), and DVB. Their basic structures and molecular weights are shown in Table III. These monomers were selected on the basis of their high vinyl functionality (4 and 2, respectively) and a relatively low molecular weight. The vinyl functionality is necessary to crosslink with the rubber (poly(*cis*-isoprene)) during the vulcanization process currently used in the fabrication of commercial tires by Bridgestone, America. The mechanism of crosslinking of natural rubber using sulfur is well known and involves a hydride abstraction step and also an addition to a double bond in the backbone chain.[30,31] Therefore, the compounds are chosen such that the vinyl groups can take part in the crosslinking mechanism, thus increasing crosslinking density at, near, and potentially under the subsurface of the fiber–rubber interface.

Further, the low molecular weight and small size (relative to the subsurface voids[27]) of these compounds enhances their solubility $scCO_2$ for monomer transport into subsurface voids created by the pretreatment processes.[32,33] The effect of $scCO_2$ on such high performance fiber's strength has been studied and shown to have no detrimental effect.[28,29] Once the uncured rubber is brought in contact with the fibers and the high concentration of vinyl groups near this region is expected to cause a locally higher crosslink density at the fiber matrix interface. This, in turn, can produce an interphase region with a gradient in modulus near the fiber as well as provide a mechanism of mechanical interlocking resulting from crosslinking within embedded regions of the fiber.

To study the effect of the addition of reactive monomers on the properties of the matrix, a sample of rubber was first soaked in excess of DVB for a period of one hour over which significant swelling of the rubber was observed. This swollen rubber was subsequently cured using conditions similar to the that for making the composites and dynamical mechanical analysis (DMA) was done to study the effect of the coupling agent on the mechanical properties of the rubber. Comparative plots of the storage modulus obtained by dynamic mechanical analysis are shown in Figure 6. Note that, a significant increase in both storage modulus and stiffness (see Figure 6) indicates that the DVB reacts and increases the crosslink density of the matrix as measured by the storage modulus of the rubber.

Adhesion Test Design

A fiber bundle pull-out test was deemed the most direct way to evaluate the interfacial adhesion between the fiber and matrix. In order to insure an appropriate embedded length necessary to

Table III. Coupling Agents

	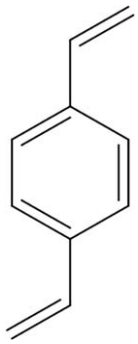	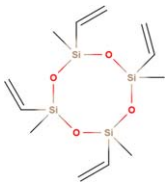	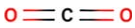
Molecular weight (g/mol)	130	345	44
Size (nm)	0.9	1	0.24

generate a uniform shear stress at the interface, modeling of the fiber bundle pull-out test was done. Simple analysis of the shear forces acting on the interface can be done using a Kelly Tyson[34] approach (see Figure 7) (Notation in Appendix A). However, a fundamental assumption in the Kelly Tyson model is that the shear stress is uniform and constant along its length which is a factor that needs to be verified.

For simplicity, we approximate the fiber bundle with a single fiber of equivalent diameter and consider a more refined shear lag model similar to that introduced by Cox[35] and later developed by others.[36–38] These models take into consideration the moduli of the matrix and the fiber along with other geometric and boundary conditions to determine what the shear stress distribution is along the fiber bundle interface. The derivation and solution for our test geometry is outlined in Appendix A with the interfacial shear stress described by eq. (1), and normal stress in the fiber by eq. (2):

$$\sigma(x)=\frac{\sigma_0 \sinh\left(\frac{nx}{R}\right)}{\sinh\left(\frac{nL}{R}\right)} \tag{1}$$

$$\tau(x)=\frac{n\sigma_0}{2}\cosh\left(\frac{nx}{R}\right) cosech\left(\frac{nL}{R}\right) \tag{2}$$

where R is the radius of fiber/bundle; σ_0, the maximum tensile stress in fiber; $\sigma(x)$, the tensile stress in the fiber as a function of x; L, the embedded length; $\tau(x)$, the interfacial shear stress as a function of x; G_m, the shear modulus of matrix; E_f, the Young's modulus of fiber; and n is $\sqrt{\frac{2G_m}{E_f \ln\left(\frac{r_o}{R}\right)}}$.

The predictions of the tensile stress and shear stress distributions as a function of embedded distance normalized by embedded length (x/L), and ratio of the fiber tensile modulus to matrix shear modulus are plotted for various values of $\left(\frac{E_f}{G_m}\right)$ in Figure 8.

The results show that as the modulus of the matrix drops in comparison to the fiber, the stress distributions move from a hyperbolic to a more linear behavior. That is, the predictions of the more advanced shear lag model and that of the Kelly Tyson

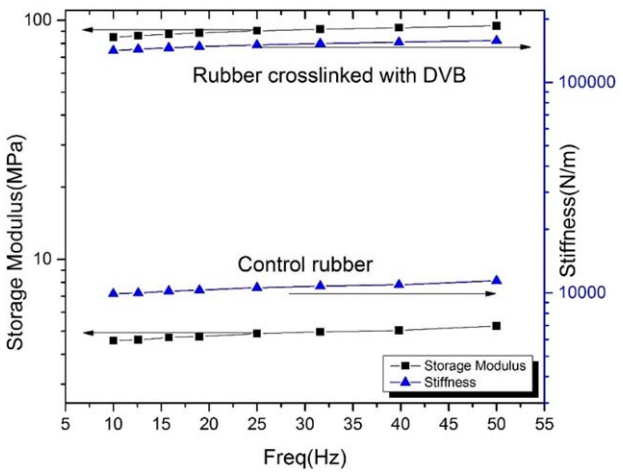

Figure 6. DMA on control rubber and rubber crosslinked with DVB. [Color figure can be viewed at wileyonlinelibrary.com]

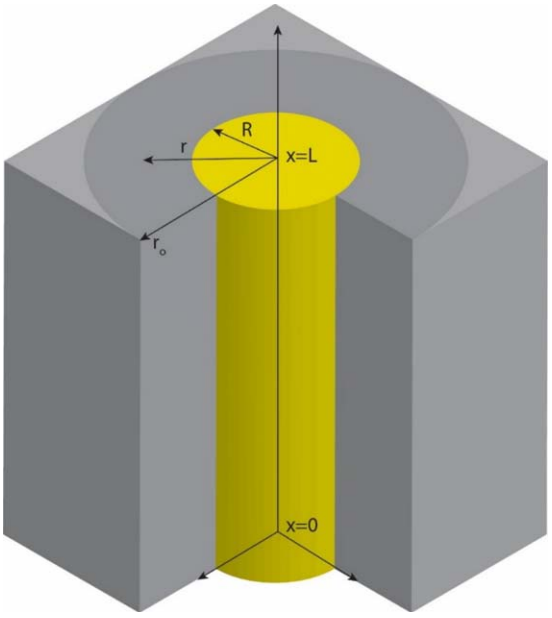

Figure 7. Cylindrical coordinate system for shear lag models showing fiber (yellow) embedded in rubber matrix. [Color figure can be viewed at wileyonlinelibrary.com]

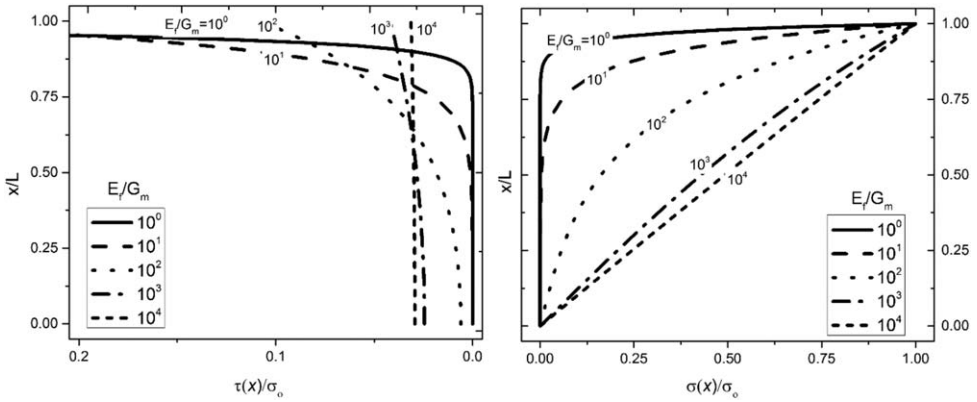

Figure 8. Tensile and shear stresses on the fiber plotted for various values of E_f/G_m over the normalized embedded length.

model converge and the modulus mismatch increases. More importantly, for our case the shear modulus of the rubber in our system is at least four orders of magnitude smaller than the tensile modulus of PPTA fibers. Consequently, we can be assured that the shear stress distribution is uniform for our embedded length of 10 mm.

Fiber matrix adhesion tests were performed on control and treated fibers with an embedded fiber bundle length of 10 mm. Figure 9 shows the results for fibers conditioned with each reactive monomer that was infused using $scCO_2$ and under ambient conditions.

The results indicate that both DVB and D4V improve the adhesion by about a 100%. DVB seems to provide better adhesion that D4V. However, the impact of $scCO_2$ on the adhesion cannot be ascertained from these tests. Further studies would be needed to get a better understanding of this.

Additional adhesion tests were performed on the fibers that were first subjected to either the microwave or mechanical pretreatments. For these tests, the fibers where subsequently treated with performed DVB as the reactive monomer since it showed the best results in Figure 9. The results from these adhesion tests are shown in Figure 10. The results indicate that both pretreatments enhance adhesion of the fibers to the matrix. The microwave treatment provides about a 10% improvement in adhesion while the mechanical treatment provides a 20% improvement.

After the adhesion tests were complete, the fiber bundles were examined using a scanning electron microscope (SEM) to evaluate the mode of failure. Results from this investigation are shown typically in Figure 11.

Note in Figure 11 that the control fibers are bare, with very little or no rubber adhering to the fiber surface, indicative of poor adhesion. In contrast, the fibers treated with DVB (no pretreatment) in the presence of $scCO_2$ show rubber adhering to the fiber, indicating a departure from interfacial failure to fracture of the rubber matrix. In addition, some fractured fibers are also visible, indicating that the strength of the fibers is being utilized to a larger extent. This image provides evidence for the creation of the interphase region that may have a locally higher crosslink density that that of the rubber away from the fiber. This interphase region results from the increase crosslink density obtained from the reactive monomers infused into the fibers.

Although more detailed studies beyond the scope of the current investigation would be required to actually characterize this interphase region, the Cox shear lag model can be easily extended to accommodate an interphase region. For completeness, we also provide for this solution in Appendix A. For this analysis, we

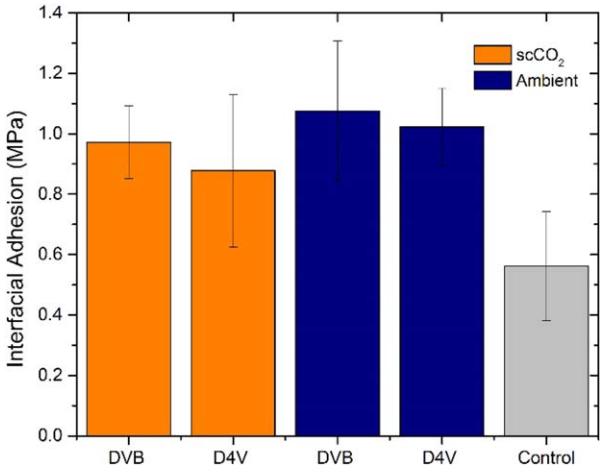

Figure 9. Adhesion of control fibers treated with different reactive monomers. [Color figure can be viewed at wileyonlinelibrary.com]

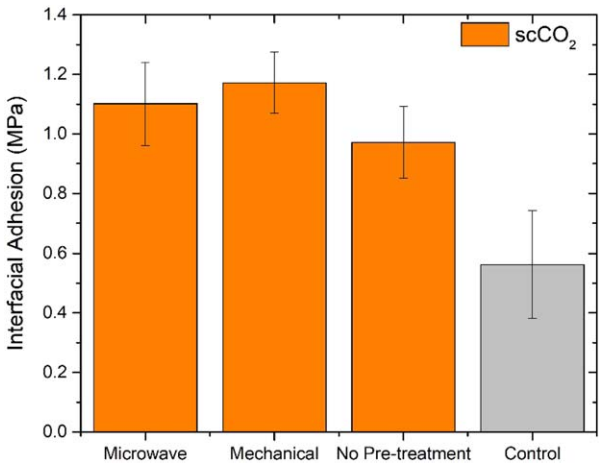

Figure 10. Effect of pretreatments on adhesion (coupling agent: DVB). [Color figure can be viewed at wileyonlinelibrary.com]

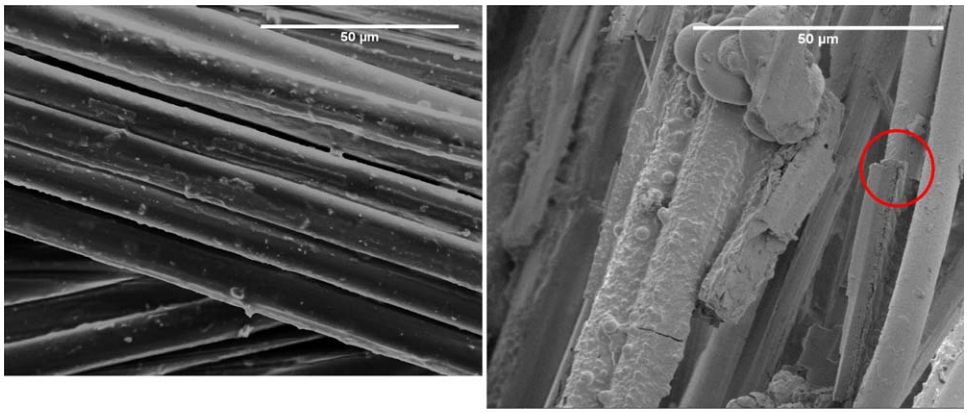

Figure 11. Failure interface of control (left) versus treated fiber indicate a suppression of interfacial failure after treatment (fractured fiber encircled). [Color figure can be viewed at wileyonlinelibrary.com]

consider an annular interphase region beginning at the fiber interface to an intermediate radius r_1 between the fiber radius R and the distance between fiber axis to tab surface r_o having a modulus higher than that of the bulk. Assuming the interphase to have a modulus of G_{m1} and the bulk to have a modulus of G_{m2}, an equivalent shear modulus can be defined as in eq. (3):

$$G_{meq}=\frac{\ln\left(\frac{r_o}{R}\right)}{\left[\frac{\ln\left(\frac{r_1}{R}\right)}{G_{m1}}+\frac{\ln\left(\frac{r_o}{r_1}\right)}{G_{m2}}\right]} \tag{3}$$

For an interphase region having an $E_f/G_{m1}=10^1$ and a bulk having an $E_f/G_{m2}=10^2$, the predictions are plotted in Figure 13. The results are compared to single stage models with bulk moduli having the ratio $E_f/G_{m1}=10^1$ and $E_f/G_{m2}=10^2$.

The two-stage model predicts that the decay of shear stresses with embedded length is more severe as compared to a system with no stiffer interphase region. This modification can be extended to include more than two phases to better explain systems that have a more gradual change in properties from interface to bulk.

A more detailed characterization of the interphase region is possible but would be quite involved and may include different analytical techniques for each of the modifications presented. The primary focus of these studies would be to directly or indirectly evaluate the stiffness and strength profile radially outward from the fiber center through the interphase region and into the matrix. This may involve a range of experimental and modeling studies. This effort is beyond the scope of what was presented in this communication and part of a future study.

CONCLUSIONS

This research has shown that the adhesion between PPTA fibers and tire rubber can be effectively doubled through a combination of fiber pretreatments and infusion of reactive monomers. New fiber pretreatments including a microwave and mechanical treatment are introduced with each showing unique alteration in the fiber morphology that enhances monomer permeation and fiber–matrix adhesion. These pretreatments are combined with two reactive monomers D4V and DVB provide superior adhesion with treatments with immersion of these monomers in the presence of $scCO_2$ having a secondary effect. Shear lag analysis was used to evaluate the test method and geometry. The results of the adhesion tests show that the coupling agents are the major contributor to improvement in adhesion, leading to an almost 100% improvement in adhesion. Microwave and mechanical pretreatments are found to be secondary contributors to adhesion leading

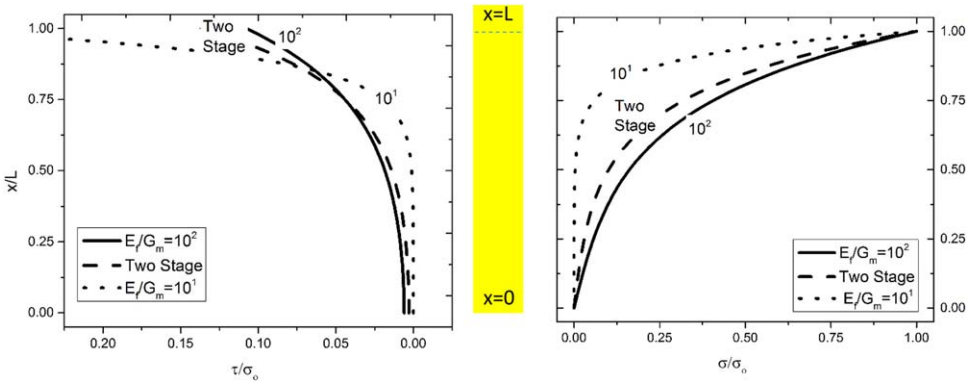

Figure 12. Two-stage model predictions. [Color figure can be viewed at wileyonlinelibrary.com]

to a 10% and 20% improvement in adhesion respectively. Failure analysis indicates a shift of failure mechanism and a suppression of interfacial failure. There is also indication of formation of an interphase region surrounding the fiber. Finally, a two-stage modification for the shear lag model is proposed to take into account the presence of the interphase region.

ACKNOWLEDGMENTS

The authors acknowledge Bridgestone Americas for their financial support, materials, and thoughtful discussions.

APPENDIX A

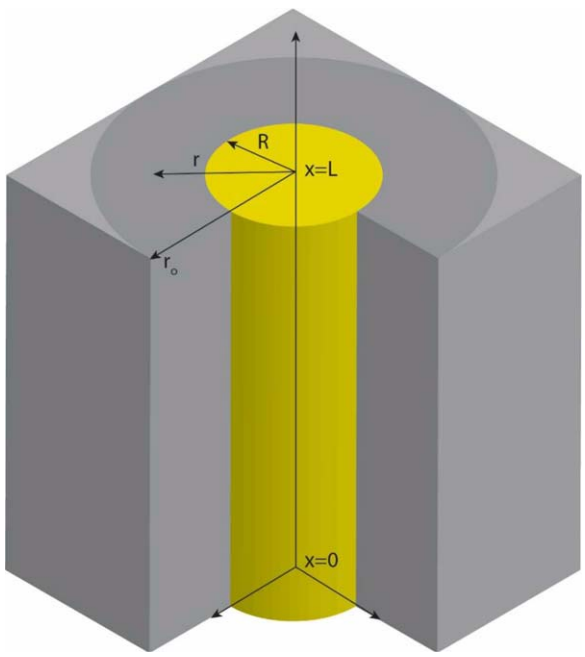

F	maximum pull-out force
R	radius of fiber/bundle
σ_0	maximum tensile stress in fiber
$\sigma(x)$	tensile stress in the fiber as a function of x
L	embedded length
$\tau(x)$	interfacial shear stress as a function of x
r	arbitrary radius
r_1	radius of interphase region
r_o	distance from fiber axis to tab surface
E_f	Young's modulus of fiber
G_{m1}	shear modulus of interphase
G_{m2}	shear modulus of matrix

First, we define a cylindrical co-ordinate system as above. The notations are described.

A force balance on an annular region surrounding the fiber gives

$$\tau_R.2\pi R dx = \tau_r.2\pi r dx$$

$$\tau_r = \frac{R}{r}.\tau_R$$

$$\frac{\delta u}{\delta r} = \gamma = \frac{\tau_r}{G_m} = \frac{\tau_R}{G_m}\left(\frac{R}{r}\right)$$

$$\int_{u_R}^{u_r} \delta u = \frac{\tau_R R}{G_m}\int_R^r \frac{1}{r}\delta r$$

$$u_r - u_R = \frac{\tau_R R}{G_m}\ln\frac{r}{R} \tag{A.1}$$

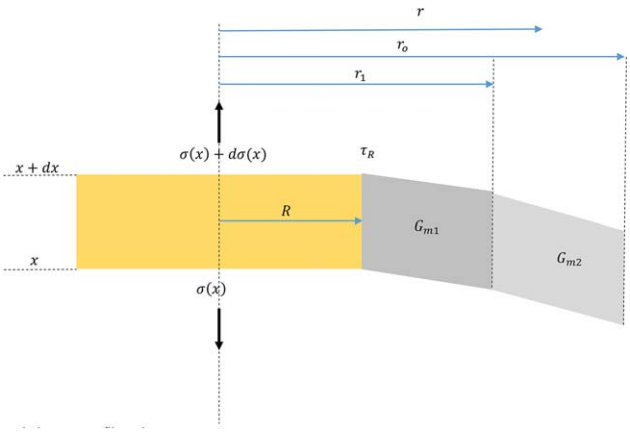

Force balance on a fiber element

$$2\pi R\tau_R dx = -\pi R^2 d\sigma(x)$$

$$-\frac{2\tau_R}{R} = \frac{d\sigma(x)}{dx}$$

Substituting from eq. (A.1), we get

$$\frac{d\sigma(x)}{dx} = \frac{2G_m(u_r - u_R)}{R^2\ln\left(\frac{r}{R}\right)} \tag{A.2}$$

Differentiating eq. (A.2), we get a second order ODE as in eq. (A.3):

$$\frac{d^2\sigma(x)}{dx^2} + \frac{n^2}{R^2}\sigma(x) = 0 \tag{A.3}$$

where

$$\frac{du_R}{dx} = \frac{\sigma(x)}{E_f}$$

and

$$n = \sqrt{\frac{2G_m}{E_f\ln\left(\frac{r_o}{R}\right)}}$$

Solving eq. (A.3), we get eq. (A.4):

$$\sigma(x) = \frac{\sigma_o\sinh\left(\frac{nx}{R}\right)}{\sinh\left(\frac{nL}{R}\right)} \tag{A.4}$$

For the two-stage shear lag model, displacement is alternatively defined as in eq. (A.5):

$$\int_{u_R}^{u_r}\delta u = \frac{\tau_R R}{G_m}\left(\int_R^{r_1}\frac{1}{r}\delta r + \int_{r_1}^{r}\frac{1}{r}\delta r\right) \tag{A.5}$$

Thus, we get an equivalent shear modulus defined in eq. (A.6):

$$G_{meq} = \frac{\ln\left(\frac{r}{R}\right)}{\left[\frac{\ln\left(\frac{r_1}{R}\right)}{G_{m1}} + \frac{\ln\left(\frac{r}{r_1}\right)}{G_{m2}}\right]} \quad (A.6)$$

This can be substituted in place of G_m to find the value of n which can then be used with eq. (A.3).

APPENDIX B

GUINIER ANALYSIS

Small-angle X-ray scattering was used to study the effect of pretreatments on void sizes. Figure 13 shows the SAXS patterns of control and treated fibers. Performing a Guinier analysis and fitting to eq. (B.1) (Figure B.1), we get void sizes of 54, 56, and 46 nm for control, mechanical and microwave pretreated fibers, respectively (Table I):

$$\log_{10} I(S) = -\frac{4\pi^2 S^2}{5}(a)^2 \log_{10} e + \text{constant} \quad (B.1)$$

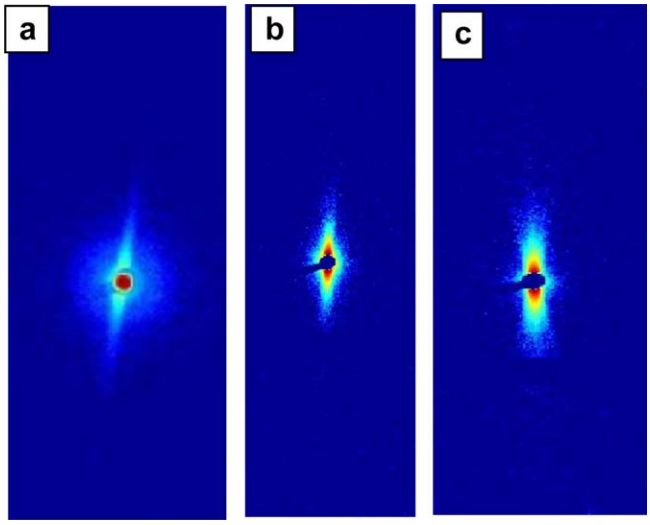

Figure 13. SAXS images of (a) control, (b) mechanical, and (c) microwave pretreated fibers. [Color figure can be viewed at wileyonlinelibrary.com]

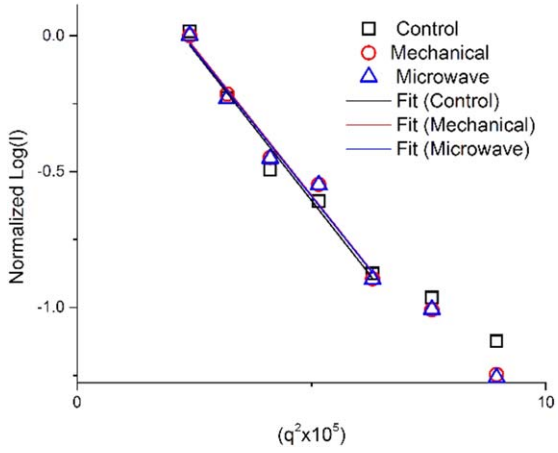

Figure B.1. Guinier analysis and fit. [Color figure can be viewed at wileyonlinelibrary.com]

REFERENCES

1. Cheng, M.; Chen, W.; Weerasooriya, T. *J. Eng. Mater. Technol.* **2005**, *127*, 197.
2. Dobb, M. G.; Johnson, D. J.; Saville, B. P. *J. Polym. Sci. Polym. Phys. Ed.* **1977**, *15*, 2201.
3. Dobb, M. G.; Johnson, D. J.; Saville, B. P. *J. Polym. Sci. Polym. Symp.* **1977**, *58*, 237.
4. Li, S. F. Y.; McGhie, A. J.; Tang, S. L. *Polymer (Guildf).* **1993**, *34*, 4573.
5. Dobb, M. G.; Hindeleh, A. M.; Johnson, D. J.; Saville, B. P. *Nature* **1975**, *253*, 189.
6. Panar, M.; Avakian, P.; Blume, R. C.; Gardner, K. H.; Gierke, T. D.; Yang, H. H. *J. Polym. Sci. Polym. Phys. Ed.* **1983**, *21*, 1955.
7. Drzal, L. T.; Rich, M. J.; Lloyd, P. F. *J. Adhes.* **1983**, *16*, 1.
8. Drzal, L. T.; Rich, M. J.; Koenig, M. F.; Lloyd, P. F. *J. Adhes.* **1983**, *16*, 133.
9. Theocaris, P. The Mesophase Concept in Composites, **2012**.
10. Benrashid, R.; Tesoro, G. C. *Text. Res. J.* **1990**, *60*, 334.
11. Yue, C. Y. Y.; Padmanabhan, K. *Compos. Part B: Eng.* **1999**, *30*, 205.
12. Takayanagi, M.; Ueta, S.; Lei, W.-Y.; Koga, K. *Polym. J.* **1987**, *19*, 467.
13. Takayanagi, M.; Kajiyama, T.; Katayose, T. *J. Appl. Polym. Sci.* **1982**, *27*, 3903.
14. Chen, M.-L.; Ueta, S.; Takayanagi, M. *Polym. J.* **1988**, *20*, 673.
15. Wertheimer, M. R.; Schreiber, H. P. *J. Appl. Polym. Sci.* **1981**, *26*, 2087.
16. Wu, G. M. *Mater. Chem. Phys.* **2004**, *85*, 81.
17. Park, J.-M.; Kim, D.-S.; Kim, S.-R. *J. Colloid Interface Sci.* **2003**, *264*, 431.
18. Lin, J. S. *Eur. Polym. J.* **2002**, *38*, 79.
19. Iyengar, Y. *J. Appl. Polym. Sci.* **1978**, *22*, 801.
20. Kalantar, J.; Drzal, L. T. *J. Mater. Sci.* **1990**, *25*, 4186.
21. Kanbargi, N.; Lesser, A. J.; Zhao, W.; Agarwal, S. P.; Rackaitis, M. WO 2017/031308 (**2017**).
22. Deteresa, S. J.; Allen, S. R.; Farris, R. J.; Porter, R. S. *J. Mater. Sci.* **1984**, *19*, 57.
23. Greenwood, J. H.; Rose, P. G. *J. Mater. Sci.* **1974**, *9*, 1809.
24. Sinclair, D. *J. Appl. Phys.* **1950**, *21*, 380.
25. Drzal, L.; Fukushima, H. U.S. Pat. 10/659,577 (**2003**).
26. Northolt, M. G. *Eur. Polym. J.* **1974**, *10*, 799.
27. Dobb, M. G.; Johnson, D. J.; Majeed, A.; Saville, B. P. *Polymer (Guildf).* **1979**, *20*, 1284.
28. Walsh, P. J.; Hu, X.; Cunniff, P.; Lesser, A. J. *J. Appl. Polym. Sci.* **2006**, *102*, 3517.
29. Walsh, P. J.; Hu, X.; Cunniff, P.; Lesser, A. J. *J. Appl. Polym. Sci.* **2006**, *102*, 3819.
30. Chaikumpollert, O.; Yamamoto, Y.; Suchiva, K.; Kawahara, S. *Polym. J.* **2012**, *44*, 772.
31. Akiba, M. *Prog. Polym. Sci.* **1997**, *22*, 475.
32. Eastman, S. A.; Lesser, A. J.; McCarthy, T. J. *J. Mater. Sci.* **2009**, *44*, 1275.

33. Eastman, S. A.; Lesser, A. J.; McCarthy, T. J. *J. Appl. Polym. Sci.* **2008**, *109*, 3961.
34. Kelly, A.; Tyson, W. R. *J. Mech. Phys. Solids.* **1965**, *13*, 329.
35. Cox, H. L. *Br. J. Appl. Phys.* **1952**, *3*, 72.
36. Lawrence, P. *J. Mater. Sci.* **1972**, *7*, 1.
37. Greszczuk, L. B. In Interfaces Compos., ASTM International: West Conshohocken, PA, **1969**; p 42.
38. Takaku, A.; Arridge, R. G. C. *J. Phys. D: Appl. Phys.* **2002**, *6*, 2038.